

INCORPORATION OF THE ARTICULATED BODY ALGORITHM INTO A MODEL-BASED SLIDING-MODE CONTROLLER FOR THE REDUCTION OF DYNAMIC COUPLING IN UNDERWATER-MANIPULATOR SYSTEMS

Serdar Soylu, Bradley J. Buckham*, and Ron P. Podhorodeski

Department of Mechanical Engineering,
University of Victoria, P.O. Box 3055, Victoria, B.C., Canada, V8W 3P6
{serdar, bbuckham, podhoro}@me.uvic.ca

*Corresponding author: Fax: (250) 721-6051

ABSTRACT

A control scheme is presented for reducing dynamic coupling between an underwater robotic vehicle (**URV**) and a manipulator. During task execution the torques commanded at the manipulator joints lead to reactions at the junction point of the manipulator and vehicle. These reactions disturb the vehicle position and orientation and are the source of the vehicle-manipulator coupling. In many underwater robotic vehicle-manipulator (**URVM**) applications, the URV serves as a base while the manipulator performs a required task. Therefore, it is necessary to hold the URV as stationary as possible. In the current work, Slotine's sliding mode control approach is used to reduce the dynamic effect of the underwater manipulator on the URV. The articulated body (**AB**) algorithm is used both for the time-domain simulation of the system and for the dynamic equations within the model-based sliding-mode controller. The AB algorithm is preferred for the time-domain system simulation, as it provides a computationally efficient simulation scheme. Finally, a three DOF manipulator mounted on a URV is considered, and results of time-domain numerical simulations of the proposed control scheme are presented.

INCORPORATION DE L'ALGORITHME DU CORPS ARTICULÉ DANS LA MODÉLISATION D'UN CONTRÔLEUR POUR LA RÉDUCTION DU COUPLAGE DYNAMIQUE DANS LES SYSTÈMES DE MANIPULATEUR DE VÉHICULE SOUS- MARIN ROBOTISÉ

RÉSUMÉ

Un schéma de contrôle est présenté pour réduire le couplage dynamique entre un véhicule sous-marin robotisé (**URV**, Underwater Robotic Vehicle) et un manipulateur. Lors de l'exécution de la tâche, les couples commandés aux articulations entraînent des réactions au point de jonction du manipulateur et du véhicule. Ces réactions perturbent la position du véhicule ainsi que son orientation et sont la source du couplage véhicule-manipulateur. Dans de nombreuses applications de manipulateur de véhicule sous-marin robotisé (**URVM**, Underwater Robotic Vehicle-Manipulator), le véhicule sert de base tandis que le manipulateur accomplit la tâche désirée. Il est donc nécessaire de maintenir le véhicule aussi stable que possible. L'approche de contrôle du mode de glissement de Slotine est utilisée pour réduire l'effet dynamique du manipulateur sous-marin sur le véhicule. L'algorithme du corps articulé (**AB**, Articulated Body) est utilisé à la fois pour l'espace temporel de la simulation du système et pour les équations dynamiques au sein de la modélisation du contrôleur du mode de glissement. L'algorithme "AB" est privilégié pour la simulation du système en espace temporel, car il fournit un schéma de simulation efficace en matière de calculs. Pour conclure, un manipulateur à trois degrés de liberté monté sur un "URV" est pris en considération, et les résultats de la simulation numérique du schéma de contrôle proposé sont présentés.

1 INTRODUCTION

URVs equipped with robotic manipulators have an important role in a number of shallow and deep-water missions for marine science, oil and gas survey, exploration recovery, and military service [1]. In these applications, URV's are used as mobile platforms that deliver robotic tools to a subsea work site.

In many URV applications, a master-slave configuration is used to operate the manipulator. In this configuration, the larger slave arm duplicates the movement of a smaller master arm driven by an operator on the surface vessel [2]. However, when the movement is replicated by the larger-slave arm, the inertial and hydrodynamic drag associated with the manipulator links create reactions at the manipulator – vehicle junction. The reaction loads perturb the vehicle attitude, heading and position and these changes in the vehicle's state act as disturbances to the placement of the end effector [2]. Furthermore, the system dynamics are highly nonlinear and vary greatly with changes in arm and vehicle orientation [3]. Consequently, reducing the effect of the dynamic coupling between the vehicle and manipulator becomes a challenging problem in obtaining better URVM performance [4].

In order to hold the URV reasonably stationary during manipulator operation, either additional manipulators are mounted on the front of the URV or an attachment system such as suction feet is used in typical URVM systems. The former option requires coordination of multiple manipulators and can make the task more difficult. The latter option uses additional mechanical units that lock themselves to the work piece structure. However, the attachment systems have some compliance and are themselves disturbed by ocean currents and manipulator motions.

Using a controller to keep the URV stationary can eliminate the need to implement additional mechanisms. A controller thus reduces the complexity of the system structure and preserves valuable payload space on the vehicle. Dunnigan and Russell [1] address the dynamic coupling problem for URVM systems, and propose the sliding-mode approach with a feedforward compensation term to minimize the URV-manipulator dynamic interactions. It is also shown that such a feedforward term significantly improves the trajectory tracking performance of the system. Ryu *et al.* [3] considers a force/torque sensor mounted at the base of the manipulator in order to detect & compensate the dynamic coupling effect. It is also shown by Ryu that in the case that such a sensor is not available, a disturbance observer is feasible. However, the practical implementation of such algorithms is not trivial [5].

The primary objective of this work is to propose a control law that reduces the dynamic coupling between the URV and the manipulator. In order to accomplish this goal, it is required to have a complete nonlinear time-domain simulation of the URVM that provides not only a test-tool for validation of the control laws to be implemented, but also a basis from which the controller model is constructed. In the current work, the AB algorithm is chosen considering that it is the most computationally efficient simulation algorithm for serial-chain structures with the number of degree of freedom (**DOF**) more than 3 [6]. Further, the AB algorithm facilitates direct calculation of the manipulator dynamic effects on the URV.

The URVM dynamics are dominated by hydrodynamic terms and it is difficult to accurately measure or estimate the hydrodynamic coefficients. This calls for a robust controller: one that is insensitive to inaccuracies in the dynamic model of the URVM. It has been shown that the sliding mode approach is an effective technique for the control of URVM systems [1], [7]. As such, in the present work the sliding-mode approach is chosen.

The remainder of the paper is outlined as follows: Section 2 describes the system, including hydrodynamic terms and thruster dynamics, and the frame attachment procedure. Section 3 explains the AB algorithm for URVM systems. Section 4 summarizes the solution procedure of the dynamics of the URVM. Section 5 explains the inclusion of the AB formulation into a sliding-mode control algorithm. Section 6 presents the simulation results and the paper finishes with conclusions in Section 7.

2 SYSTEM DESCRIPTION AND FRAME ATTACHMENT

In this section the complete dynamic model of the URVM system is presented. Existing dynamics models of URVMs include that of Ioi and Itoh [8] who extended the Newton-Euler formulation to include

the requisite hydrodynamics terms, and Tarn *et al.* [10] who developed a dynamic model of a URVM based on Kane's method. McMillan *et al.* [9] extended the AB formulation to develop a computationally efficient dynamic simulation of a URVM system. The current work follows the developments of [9].

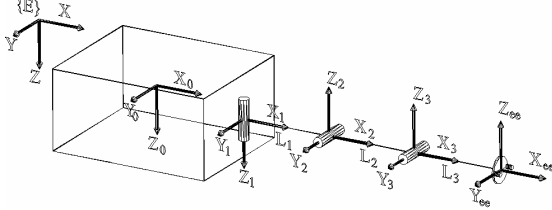


Figure 1: Frame Attachments for the URVM System

Table 1: D&H Parameters for the Manipulator

$i-1$	$\alpha-1$	a_{i-1}	d_i	θ_i	i
0	0	0	0	q_1	1
1	$-\pi/2$	L_1	0	q_2	2
2	0	L_2	0	q_3	3
3	0	L_3	0	0	ee

As shown in Figure 1, the Z axis of the earth-fixed inertial frame $\{E\}$ is assumed in the gravity direction as is consistent with traditional marine mechanics. The URV is modeled as another manipulator link in the serial chain and numbered as 0. The body-fixed frame is attached to the centre of mass of the URV as shown in Figure 1. The URV spatial velocity state vector with respect to (**wrt**) its body-fixed frame is considered to be $\mathbf{v} = [\boldsymbol{\omega}_0^T \ \mathbf{v}_0^T]^T = [p \ q \ r \ u \ v \ w]^T$, and the position and orientation state vector of the URV wrt the inertial frame is given by $\mathbf{x} = [\phi \ \theta \ \psi \ X \ Y \ Z]^T$. The spatial transformation matrix between the inertial frame and URV's body-fixed frame is given by \mathbf{T} , which includes the angular velocity transformation matrix \mathbf{T}_2 and the linear velocity transformation matrix \mathbf{T}_1 . \mathbf{T} can be obtained by the Euler sequence of rotations: the first rotation ψ is about the Z axis of the inertial frame (yaw), the second rotation θ is about the new Y axis (pitch), and finally, the last rotation ϕ is about the new X axis (roll);

$$\dot{\mathbf{x}} = \mathbf{T}\mathbf{v}, \quad \mathbf{T} = \begin{bmatrix} \mathbf{T}_2 & \mathbf{0}_{3 \times 3} \\ \mathbf{0}_{3 \times 3} & \mathbf{T}_1 \end{bmatrix},$$

$$\mathbf{T}_2 = \begin{bmatrix} 1 & s\phi t\theta & c\phi t\theta \\ 0 & c\phi & -s\phi \\ 0 & s\phi/c\theta & c\phi/c\theta \end{bmatrix}, \quad \mathbf{T}_1 = \begin{bmatrix} c\psi c\theta & -s\psi c\phi + c\psi s\theta s\phi & s\psi s\phi + c\psi s\theta c\phi \\ s\psi c\theta & c\psi c\phi + s\psi s\theta s\phi & -c\psi s\phi + s\psi s\theta c\phi \\ -s\theta & c\theta s\phi & c\theta c\phi \end{bmatrix}, \quad (1)$$

$$s \equiv \sin(*), \quad c \equiv \cos(*), \quad t \equiv \tan(*).$$

With regards to the manipulator part of the URVM, the body-fixed frames are labelled from 1 through ee, with ee representing the end-effector. The body-fixed frames are attached to a base joint of each successive link using the modified Denavit-Hartenberg convention [11] and as shown in Figure 1 and Table 1. The joint position state vector for the manipulator is defined by $\mathbf{q} = [q_1 \ q_2 \ q_3]^T$, where q_i is the rotation angle of the i^{th} joint. The rotation matrices from link to link can be obtained from homogeneous transforms based on the modified Denavit-Hartenberg parameters.

2.1 Hydrodynamic Effects for Rigid Body Dynamics

The nonlinear hydrodynamic forces acting over a URVM system have been identified by Ioi and Itoh [8] as added mass, viscous drag, fluid acceleration and buoyancy.

2.1.1 Added Mass

When a submerged body accelerates through a fluid, an additional inertial resistance occurs. This additional inertial effect can be characterized by a 6×6 symmetric positive definitive added mass matrix. If the body is symmetric and moves slowly, the contribution of the off-diagonal elements in the added mass matrix can be neglected. In the event that experimental values are not available, these coefficients can be estimated by using strip theory. In the current work, the URV is approximated as a cube and the manipulator links are approximated as cylinders. The derivation of the added mass coefficients using strip theory for the cubic vehicle approximation is shown by Fossen [12] and the coefficients for the cylindrical

manipulator links are given by Patel [13]. Note that added mass contribution due to accelerations along the length of the cylinder is assumed to be negligible.

Newman [14] derived added mass force and moment equations for a rigid body and these expressions have been written in a form consistent with the AB algorithm proposed by McMillan *et al.* [9], as follows:

$$\mathbf{f}_i^A = -\mathbf{I}_i^A \mathbf{a}'_i + \boldsymbol{\beta}_i^A = -\mathbf{I}_i^A \begin{bmatrix} \dot{\boldsymbol{\omega}}_i \\ \mathbf{a}'_i \end{bmatrix} + \mathbf{I}_i^A \begin{bmatrix} \mathbf{0}_{3 \times 1} \\ (\mathbf{a}_f - \mathbf{a}_g) + \boldsymbol{\omega}_i \times \mathbf{v}_i^r \end{bmatrix} - \begin{bmatrix} \tilde{\boldsymbol{\omega}}_i & \tilde{\mathbf{v}}_i^r \\ \mathbf{0}_{3 \times 3} & \tilde{\boldsymbol{\omega}}_i \end{bmatrix} \mathbf{I}_i^A \begin{bmatrix} \boldsymbol{\omega}_i \\ \mathbf{v}_i^r \end{bmatrix} \quad i = 0 \dots 3 \quad (2)$$

where \mathbf{f}_i^A is a 6×1 vector expressed in the body-fixed frame combining a 3×1 force and a 3×1 torque vector, and \mathbf{I}_i^A is the added mass matrix of the i^{th} link. $\boldsymbol{\beta}_i^A$ is a 6×1 bias force vector combining all velocity dependent terms of the added mass force. The angular acceleration and translational biased acceleration are represented by $\dot{\boldsymbol{\omega}}_i$ and \mathbf{a}'_i , respectively. The velocity of the i^{th} link wrt the surrounding fluid is defined by \mathbf{v}_i^r . Lastly, \mathbf{a}_g and \mathbf{a}_f are the body's gravitational acceleration and the surrounding fluid translational acceleration. All vectors are given in terms of the body-fixed frame. The tilde operator refers to a skew symmetric matrix formed from the components of the vector entity.

2.1.2 Drag and Lift Forces

In the present work, it is assumed that lift and lift-related forces are small enough to ignore. It is also assumed that variations in the drag coefficients over the range of the URVM workspace are negligible. The computation of drag forces for the URV and manipulator is conducted separately.

2.1.2.1 URV translational and rotational drag

Translational drag force incurred along a particular axis of the URV body fixed frame can be given by:

$$F_{0_j}^D = -\frac{1}{2} \rho A_j C_{0_j}^D \mathbf{v}_{0_j}^r \left| \mathbf{v}_{0_j}^r \right| \quad j = 4 \dots 6 \quad (3)$$

where ρ is the density of the surrounding fluid and j indicates the particular DOF of the URV. For example, $j = 1 \dots 3$ and $j = 4 \dots 6$ represents rotations about and translations along the X_0 , Y_0 and Z_0 axes respectively. With regards to the remaining terms, A_j is the frontal area of the URV face perpendicular to the j direction, $\mathbf{v}_{0_j}^r$ is the relative velocity wrt the fluid, and $C_{0_j}^D$ is the drag coefficient attributed to the perpendicular face. It is assumed that drag forces act at the centre of pressure of each face of the URV.

To compute rotational drag effect, the URV is again approximated as a cube. Each side length of the cube is divided into small strips starting at the central axis of the rotational motion and moving outward. The drag force on the face of each strip is calculated using Eq. (3) based on the strip's velocity relative to the surrounding fluid. The collective moment of these translational drag forces over the entire body can be obtained by integrating the vector product of each strip's distance from the central axis r_{strip} and the translational drag force accumulated over the strip, dF_{strip}^D . Rotational drag wrt the URV's centre of mass is given by:

$$M_{0_j}^D = 2 \int r_{strip} dF_{strip}^D \quad j = 1 \dots 3. \quad (4)$$

The spatial drag force acting on the URV is given by:

$$\mathbf{f}_0^D = [M_{0_1}^D \quad M_{0_2}^D \quad M_{0_3}^D \quad F_{0_4}^D \quad F_{0_5}^D \quad F_{0_6}^D]^T \quad (5)$$

2.1.2.2 Translational and rotational drag acting on the manipulator body

The manipulator links are approximated as cylinders. The resultant drag force \mathbf{F}_i^D and moment exerted \mathbf{M}_i^D onto i^{th} link can be found by integrating the partial drag force and moment on each strip over the length of the cylindrical link [15],

$$\mathbf{f}_i^D = \begin{bmatrix} \mathbf{M}_i^D \\ \mathbf{F}_i^D \end{bmatrix} = \begin{bmatrix} -0.5\rho C_i^D \int_0^{L_i} \|\mathbf{v}_i^n\| \left([L_i \ 0 \ 0]^T \times \mathbf{v}_i^n \right) 2r_i \cdot dl_i \\ -0.5\rho C_i^D \int_0^{L_i} \|\mathbf{v}_i^n\| \mathbf{v}_i^n 2r_i \cdot dl_i \end{bmatrix} \quad i=1\dots3 \quad (6)$$

where r_i and L_i are the radius and length of the cylindrical link i , respectively, and \mathbf{v}_i^n is the normal velocity of the link i at the location l_i relative to the surrounding fluid. We assume the tangential drag on the cylindrical link to be negligible. Note that the moment term, \mathbf{M}_i^D , is calculated with respects to the base joint of the link. This facilitates direct inclusion of Eq. (6) into the AB formulation.

2.1.3 Buoyancy and Fluid Acceleration Forces

The buoyant force of a body opposes gravity and is equal to the weight of the displaced fluid. The fluid acceleration force is proportional to the acceleration of the fluid. These two forces are combined in the following calculation:

$$\mathbf{f}_i^{TB} = m_i^f (\mathbf{a}_f - \mathbf{a}_g) \quad i=0\dots3. \quad (7)$$

where m_i^f is the mass of displaced fluid by the i^{th} link. The buoyancy and fluid acceleration forces are exerted at the body's centre of buoyancy. The spatial force is given by

$$\mathbf{f}_i^{TB} = \begin{bmatrix} \mathbf{b}_i \times \mathbf{f}_i^{TB} \\ \mathbf{f}_i^{TB} \end{bmatrix} \quad i=0\dots3, \quad (8)$$

where \mathbf{b}_i is the position vector from the body-fixed frame to the centre of buoyancy of the body.

2.2 Thruster Dynamics

It has been established that thruster dynamics are a significant effect within a URV dynamics model. Yoerger *et al.* [16] developed a dynamic thruster model for use in underwater vehicles. Although his model accurately captures the time delay between motor control signals and developed thrust, it does not account for all possible combinations of propeller rotational rate and flow direction through the thruster's shroud. Van Lammaren *et al.* [17] came up with a model that characterizes all these possible combinations through a four-quadrant mapping of the apparent angle of approach of water particles on the blades. Healey *et al.* [18] combined an armature controlled motor model, a theoretical propeller mapping using airfoil theory and a fluid momentum model applied within the finite volume of the shrouded region. Healey *et al.* [18] only considered the axial component of the fluid flow and used sinusoidal lift/drag curves. Bachmayer *et al.* [19] incorporated the effects of the rotational fluid motion on thruster response and further proposed a method to experimentally determine non-sinusoidal lift/drag curves. In the present work, Healey's approach is followed since we consider a hypothetical URVM structure for which experimental thruster data is not available. In the present work, the thrusters configuration uses two surge thrusters, that can be operated differentially for yaw motion, and a single heave thruster. According to Healey's approach, the state equations for the h^{th} thruster are given by:

$$\dot{\Omega}_h = g_1(\Omega_h, U_h^a, V_h), \quad \dot{U}_h^a = g_2(\Omega_h, U_h^a) \quad h=1\dots3 \quad (9)$$

where Ω_h is motor rotational rate, U_h^a is the axial fluid velocity at the propeller and V_h is the voltage input. The thrust contributed by the h^{th} thruster is

$$T_h = g_3(\Omega_h, U_h^a). \quad (10)$$

The vector of torques and forces acting on the centre of the mass of the URV, \mathbf{f}_0 , is given by

$$\mathbf{f}_0 = \mathbf{\Lambda} [T_1 \ T_2 \ T_3]^T \quad (11)$$

where $\mathbf{\Lambda}$ is a 6×3 thruster mapping matrix, which is dependent on the thruster position and orientation on the URV. The collective state of the thrusters is defined by the vectors:

$$\mathbf{\Omega} = [\Omega_1 \ \Omega_2 \ \Omega_3]^T, \quad \mathbf{U} = [U_1 \ U_2 \ U_3]^T. \quad (12)$$

3 ARTICULATED BODY ALGORITHM

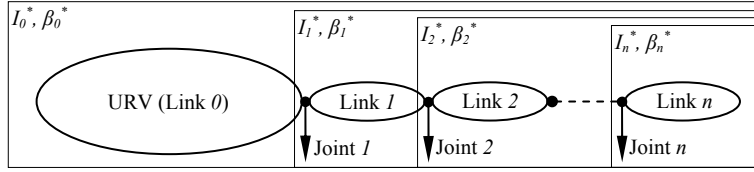


Figure 2: Serial Chain of a URVM

Figure 2 represents the model of a URVM system, which is numbered from 0 through n . The mobile base, which represents the URV, is designated as link 0 and the manipulator part of the system is indicated by numbering from 1 through n , with n including the end effector. The solid arrows indicate the joint axes between each successive link. The motion afforded by a single joint is defined by a spatial unit vector ϕ_i . The vector ϕ_i maps the contribution of the i^{th} joint rotation, a scalar value, to the spatial motion of the articulated body. The manipulator joints are single DOF revolute joints. When considering the i^{th} joint, the axis of revolution is the z_i axis and the corresponding joint axis representation is given by $[0 \ 0 \ 1 \ 0 \ 0 \ 0]^T$. The URV has a 6 DOF motion contribution to the articulated body. This contribution is defined explicitly by the vector \mathbf{v}_0 .

Figure 2 also graphically depicts the relationship between the i^{th} link and the i^{th} articulated body. The i^{th} link on its own is a rigid body whose motion is governed by Newton's 2nd law and Euler's Equations of Motion. The i^{th} articulated body is composed of links i through n and the connecting joints. The AB algorithm seeks to relate the motion of the i^{th} articulated body to joint torques applied at joint i . The overall manipulator motion is found by superposing the motion of each articulated body. The process depends on knowing the articulated inertia that is seen by the actuator at joint i .

For the hypothetical URVM considered in the present work, $n = 3$ and the articulated body inertia of the i^{th} articulated body, $\mathbf{I}_i^* \in \mathbf{R}^{6 \times 6}$, is given by:

$$\mathbf{I}_{i-1}^* = \mathbf{I}_{i-1}^H + p_1(\mathbf{I}_i^*, \phi_i) \quad i = 3 \dots 1 \quad (13)$$

where $\mathbf{I}_3^* = \mathbf{I}_3^H$ and the term $\mathbf{I}_3^H = \mathbf{I}_i + \mathbf{I}_i^A$ is the hydrodynamic inertia of the rigid i^{th} link, with \mathbf{I}_i representing the inertia tensor of that link. In addition to the articulated inertias, a bias force must be calculated for each joint i . The bias force, β_i^* , represents the force that each joint must exert to maintain the current link velocities:

$$\beta_{i-1}^* = \beta_{i-1}^H + p_2(\beta_i^*, \mathbf{I}_i^*, \phi_i, \tau_i) \quad i = 3 \dots 1 \quad (14)$$

where $\beta_3^* = \beta_3^H - {}^{ee}\mathbf{X}_3^T \mathbf{f}_{ee}$, \mathbf{f}_{ee} is a force applied at the end-effector, ${}^{ee}\mathbf{X}_3$ is a spatial transformation between the ee and link 3 coordinate systems, the term $\beta_i^H = \beta_i + \beta_i^A + \mathbf{f}_i^D + \mathbf{f}_i^{TB}$ is the hydrodynamic bias of the i^{th} link, and τ_i is the joint torque. Detailed calculation of Eq. (13) and Eq. (14) is given in [9].

3.1 The URV Dynamic Modelling

The goal of this section is to present the nonlinear motion of the URV, which includes the manipulator dynamic effects, using the AB approach [9]. The nonlinear equations of motion of the URV are given by:

$$\mathbf{f}_0 = \mathbf{I}_0^* \mathbf{a}'_0 - \beta_0^*, \quad (15)$$

$$\mathbf{a}'_0 = (\mathbf{I}_0^*)^{-1}(\mathbf{f}_0 + \beta_0^*) \quad (16)$$

where $\mathbf{I}_0^* \in \mathbf{R}^{6 \times 6}$ represents the AB inertia of the whole URVM, including the added mass inertial contributions of the each link to the articulated body. The term $\beta_0^* \in \mathbf{R}^6$ is a bias force that contains the hydrodynamic and environmental forces, excluding gravity, acting over the entire URVM. The components of the vector $\mathbf{f}_0 \in \mathbf{R}^6$ are the control forces and moments exerted by the thrusters on the URV. The term $\mathbf{a}'_0 \in \mathbf{R}^6$ is the biased acceleration vector of the URV. All vectors are expressed in terms

of the URV's body-fixed frame. In the simulation, the unbiased acceleration vector of the URV is needed. The unbiased acceleration vector \mathbf{a}_0 is:

$$\mathbf{a}_0 = \mathbf{a}'_0 + [\mathbf{0}_{1 \times 3} \quad {}^0\mathbf{a}'_g]^T = (\mathbf{I}_0^*)^{-1}(\mathbf{f}_0 + \boldsymbol{\beta}_0^*) + [\mathbf{0}_{1 \times 3} \quad {}^0\mathbf{a}'_g]^T. \quad (17)$$

The purpose of a time domain simulation of the URV is to compute the accelerations of the URV based on a current state that is defined by positions and velocities. Using the position, velocity, and acceleration values, a numerical integrator computes the next position and velocity of the system. An initial state of the system must be given in order to propagate the simulation. It is desired to know the history of vehicle positions and orientations in terms of the inertial reference frame. Therefore, the velocity and unbiased accelerations calculated from Eq. (17) are transformed from body-fixed frame to inertial frame prior to the integration step. This can be done using the following spatial transformations:

$$\dot{\mathbf{x}} = \mathbf{T}\mathbf{v}, \quad \ddot{\mathbf{x}} = \mathbf{T}\mathbf{a}_0 + \begin{bmatrix} \dot{\mathbf{T}}_2 & \mathbf{0}_{3 \times 3} \\ \mathbf{0}_{3 \times 3} & \mathbf{0}_{3 \times 3} \end{bmatrix} \mathbf{v}. \quad (18)$$

Note that without inclusion of the manipulator dynamics, the unbiased spatial acceleration calculated in (17) becomes equivalent to the one derived by Fossen [12] with the exception that the AB algorithm produces absolute translational accelerations while Fossen's solution procedure gives solutions that are wrt a body's rotating reference frame.

3.2 The Manipulator Dynamic Modelling

The force balance equation associating the control force \mathbf{f}_i provided by the manipulator's i^{th} joint with the motion of the outboard articulated links, link i through 3, is given by:

$$\mathbf{f}_i = \mathbf{I}_i^* \mathbf{a}'_i - \boldsymbol{\beta}_i^* \quad (19)$$

where \mathbf{I}_i^* represents the AB inertia of link i through 3. The term $\boldsymbol{\beta}_i^*$ is a bias force that contains the hydrodynamic and environmental forces, excluding gravity, acting on the URVM [6].

The biased acceleration of the i^{th} link is given by:

$$\mathbf{a}'_i = {}^i\mathbf{X}_{i-1} \mathbf{a}'_{i-1} + \boldsymbol{\phi}_i \ddot{q}_i + \boldsymbol{\zeta}_i \quad (20)$$

where $\boldsymbol{\zeta}_i$ is the vector of Coriolis and the centripetal accelerations of link i . For simulation purposes, the joint accelerations \ddot{q}_i $i=1 \dots 3$ are required. To obtain these joint accelerations, Eq. (20) is substituted into Eq. (19) and then force \mathbf{f}_i is projected onto the joint axis according to:

$$\tau_i = \boldsymbol{\phi}_i^T \mathbf{f}_i \quad (21)$$

The resulting equation is solved for the unknown \ddot{q}_i [6]:

$$\ddot{q}_i = (m_i^*)^{-1} \tau_i - \left[\mathbf{n}_i (m_i^*)^{-1} \right]^T \left({}^i\mathbf{X}_{i-1} \mathbf{a}'_{i-1} + \boldsymbol{\zeta}_i \right), \quad (22)$$

where

$$\mathbf{n}_i = \mathbf{I}_i^* \boldsymbol{\phi}_i, \quad m_i^* = \boldsymbol{\phi}_i^T \mathbf{I}_i^* \boldsymbol{\phi}_i, \quad \tau_i^* = \tau_i + \boldsymbol{\phi}_i^T \boldsymbol{\beta}_i^*. \quad (23)$$

4 SOLUTION PROCEDURE

The complete hydrodynamic AB algorithm for the forward dynamics problem is given in [9]. The AB hydrodynamics algorithm consists of three steps. The first step, called forward kinematics, is the computation of the velocity-dependent terms from the URV to the end effector. The first step also involves the computation of velocity dependent terms of the added mass force of Eq. (2), the drag forces of Eqs. (3), (4), and (6), and the fluid acceleration and buoyancy forces of Eq. (8) using the state of the URVM $\mathbf{X} = [\mathbf{x}^T \quad \dot{\mathbf{x}}^T \quad \mathbf{q}^T \quad \dot{\mathbf{q}}^T \quad \boldsymbol{\Omega}^T \quad \mathbf{U}^T]^T$. The second step, called backward dynamics, involves computing the articulated inertias, \mathbf{I}_i^* , $\boldsymbol{\beta}_i^*$ $i=0 \dots 3$ from the end effector to the URV based on Eq. (13) and Eq. (14). The third step, called forward acceleration, is the calculation of the accelerations of the URV, $\ddot{\mathbf{x}}$, based on Eq. (18), of the manipulator, $\ddot{\mathbf{q}}$, based on Eq. (22) and of the thruster, $\dot{\boldsymbol{\Omega}}$ and $\dot{\mathbf{U}}$, based on Eq. (9).

5 SLIDING MODE CONTROL BASED ON AB FORMULATION

The sliding mode strategy has been successfully applied to the robust control of underwater vehicles [7], [21]. The same control approach has also been implemented to URVM systems by considering the dynamic coupling between the two systems as disturbances in the vehicle control loop [1]. In [1], the URV and manipulator are modelled separately within the controller and the disturbances caused by the manipulator motion have been incorporated into the control law by introducing a feedforward compensation term that is obtained using the Newton-Euler recursive algorithm for manipulator dynamics. It has been shown that the dynamical loads transmitted from the URV to the manipulator can be incorporated in the recursive Newton-Euler equations by using the URV velocities and accelerations as the base motions of the manipulator [1]. However, this requires knowing the acceleration state knowledge of the URV, which is difficult to measure accurately during the URV operation. Therefore, it is proposed that the AB algorithm be used in the control law equations since it affords direct calculation of the URV accelerations based on a known URVM state vector \mathbf{X} . This eliminates the need to estimate the URV accelerations using inertial measurement sensors. Furthermore, since the dynamic coupling effects are embedded in the URV's AB equations, it is expected to have a better approximation of the URV dynamics at the expense of a relatively small increase in the computational complexity of the controller.

5.1 Sliding-Mode Control Law Design

This section proposes a control law based on [7]. The control law design method involves breaking the control system up into a set of low-order controllers so that each axis of the URV has a separate controller. Each controller includes cross-coupling terms due to the multi-axis motion of the URV and the manipulator dynamic effects on the URV. These coupling effects are treated as disturbances within each controller.

The dynamic model of the URV within the controller is derived from Eq. (17). The sliding mode control strategy seeks to control motion of the URV as seen by an observer in the URV's body fixed frame. Since Eq. (17) gives the absolute URV accelerations it is necessary to remove the component of this result that is due to the rotating body fixed frame. As such, the controller model is given by:

$$\mathbf{a} = (\mathbf{I}_0^*)^{-1}(\mathbf{f}_0 + \boldsymbol{\beta}_0^*) + \begin{bmatrix} \mathbf{0}_{1 \times 3} & \mathbf{0} \mathbf{a}_g^T \end{bmatrix}^T - \begin{bmatrix} \mathbf{0}_{1 \times 3} & (\boldsymbol{\omega}_0 \times \mathbf{v}_0)^T \end{bmatrix}^T \quad (24)$$

To illustrate the control law design, only the URV surge motion is described in detail. The model of the dynamics of the surge axis in the sliding-mode controller can be given as follow:

$$\dot{u} = \hat{f}(\mathbf{x}, \mathbf{v}, \mathbf{q}, \dot{\mathbf{q}}) \quad (25)$$

where \dot{u} is the time derivative of the URV's surging velocity when \mathbf{f}_0 is equal to zero, the term, $\hat{f}(\mathbf{x}, \mathbf{v}, \mathbf{q}, \dot{\mathbf{q}})$ is the estimation of this same quantity based on Eq. (24).

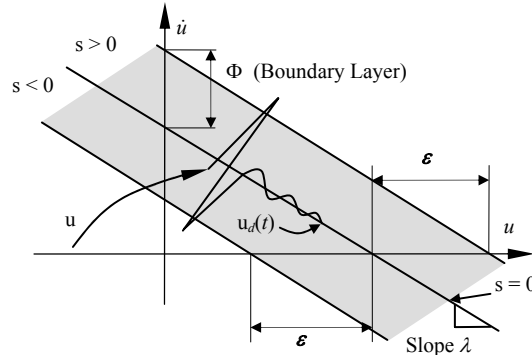


Figure 3: Sliding Surface in the State Space

The first step in the design of the controller is the definition of a surface s in the state space on which the control input is switched. This surface is called a switching surface and is used to characterize the desired dynamics. The URV surge dynamics is represented by a second-order nonlinear differential

equation, and therefore the corresponding switching surface is a line in the state space as shown in Figure 3. The switching line s for the surge motion of the URV is given by:

$$s = u_e + \lambda x_e, \quad x_e = x - x_d \quad (26)$$

where subscript e and d represents the error between the desired and current values of the corresponding state variables and the desired value of the state variable, respectively. The term x is the X_0 coordinate of the URV's absolute position. Finally, λ is the bandwidth of the closed-loop system, which is a strictly positive constant [22]. The limiting factors on the choice of control bandwidth are given in [22].

The control input u^c is chosen so that the system state is driven onto the switching line and then is kept on the line in spite of parameter changes and disturbances. Once the system state is trapped on this line, it remains on the switching line provided that the sliding condition is satisfied [7]. As a result, the system behaves consistently with the desired dynamics when sliding occurs. The control input is given by:

$$u^c = \hat{b}^{-1}[\hat{u}^c - k \text{sat}(s/\Phi)] \quad (27)$$

where

$$\hat{b} = (b_{\min} b_{\max})^{1/2}, \quad \hat{u}^c = -\hat{f} + \ddot{u}_d - \lambda \dot{u}_d, \quad k = \beta(F + \eta) + (\beta - 1)|\hat{u}^c|, \quad F = |f - \hat{f}|. \quad (28)$$

The variable \hat{b} is the estimation of the control gain b and is defined as the geometric mean of lower bound b_{\min} and upper bound b_{\max} of b . The control input is composed of two parts; the continuous part \hat{u}^c , which is model based and is the best approximation that would achieve $\dot{s} = 0$, and the discontinuous part, $k \text{sat}(s/\Phi)$, which is a nonlinear feedback component. If the dynamic model is perfect, the continuous part keeps the state on the sliding line and the state value converges to the desired point exponentially with a time constant equal to $1/\lambda$. The discontinuous term assures that the sliding condition is satisfied in the presence of model uncertainty and disturbances. The gain k is a function of the system state and possibly time. The gain k changes depending on the model uncertainties and disturbances [22]. Note that u^c is the surge component of the commanded thrust \mathbf{f}_0 . The actual URV dynamics are given by f and the estimate of f , the model dynamics, is given by \hat{f} . β is computed according to:

$$\beta = (b_{\min} / b_{\max})^{1/2}. \quad (29)$$

The value of η determines the degree to which the state of the system is attracted to the switching line [1], [22]. It is also associated with the control activity: larger η values result in higher control activity. The saturation function, $\text{sat}(\ast)$, is introduced to make the control activity continuous within the boundary layer and discontinuous outside the boundary layer. This relaxes the control law and reduces control activity at the expense of controller performance [22]. Once the system state is driven into the boundary layers, it remains in that region provided that the uncertainty bounds are not exceeded [22]. The guaranteed precision that the theory provides is [22]

$$\varepsilon \approx \Phi / \lambda. \quad (30)$$

The sliding-mode controller design involves determining the gain η so that the system state hits the sliding surface in a finite time. The discontinuous term is responsible for compensating the uncertainties in the dynamic model and it keeps the system state on the line by pushing the system state back on the line in the event of $s \neq 0$. Finally, s governs the dynamic behaviour of the state.

6 SIMULATION RESULTS

The simulation of the URVM is performed to demonstrate the effectiveness of the proposed control law on reducing the dynamic coupling in the URVM system. The URVM system considered in this work is shown in Figure 1 and all the associated parameters are given in the Appendix. In the simulation, a station keeping task is considered for the URV whose the initial orientation and position vector is $\mathbf{x} = [0 \ 0 \ 0 \ 0 \ 0 \ 0]^T$ rad, m. The initial configuration of the manipulator is taken as $\mathbf{q} = [0 \ 0 \ 0]^T$ rad. Only the URV's motion in the horizontal plane, *i.e.*, $[X \ Y \ \psi]^T$, is controlled. A randomly selected torque vectors of $\boldsymbol{\tau} = [2, 5 \ 0 \ 0]^T$ Nm and $\boldsymbol{\tau} = [0.01 \ 0 \ 0]^T$ Nm are applied to the manipulator joints

for $t \leq 2$ sec. and for $2 \leq t \leq 10$ sec., respectively. Even though these joint torque values have been chosen arbitrarily, improvement has been obtained for any joint torque values. Note that while the error in the location of the URV is limited theoretically by Eq. (30), there is no simply stated limit on the end-effector location errors. The accuracy of the end-effector path following varies depending on the specific torque values. This is largely caused by the geometry of the system: small changes in the location of the URV (base) are amplified by the link length, which causes larger errors in the location of the end effector. In order to model uncertainties in the controller, drag and added mass coefficients differed from the real system by 60%.

Figure 4 demonstrates the resulting end effector tracking path on the X-Y plane under different conditions. The first case in Figure 4, URV fixed control off, corresponds to the ideal case in which the URV is held fixed and the system behaves as a land-based manipulator. The author's consider the *ee* path of this case to represent the pilot's true intent. In the second case, URV released-control off, the URV is released with no active control. In the third case, URV released-control on, the URV is released and the control is turned on. From Figure 4, one can see that the controller works to provide a fixed-base for the manipulator by reducing the dynamic coupling between the URV and the manipulator.

The URV position error caused by the manipulator motions for the uncontrolled and controlled systems are shown in Figure 5 and Figure 6, respectively. The displacements are in terms of the URV's body fixe frame. The improvement is rather obvious in these figures. Figure 7 is the plot of the boundary layers and s , which indicates the discrepancy between the resulting motion and the desired motion. This figure shows that s remains inside the boundary layers. Figure 8 shows the forces and moments at the center of mass of the URV commanded by the controller. One can see that the commanded forces and moments are smooth and free of chattering. This is attributed to the presence of the boundary layer, which relaxes the control law within the boundary layer and in turn provides smooth control outputs. The boundary layer thickness was chosen using trial and error to ensure that chattering was not encountered by the actuators. Smaller boundary layer values can cause chattering of the thrusters shafts.

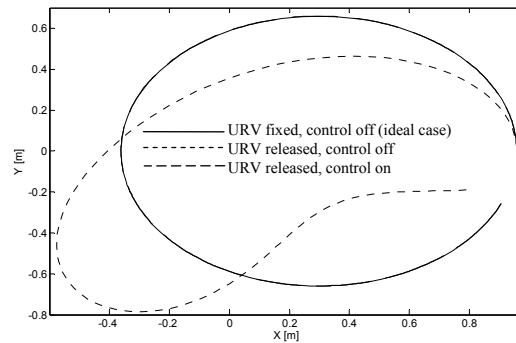


Figure 4: End-Effector Path on X-Y Plane

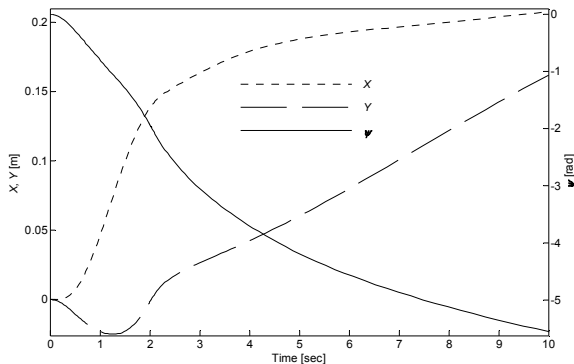


Figure 5: Uncontrolled URV Location Errors

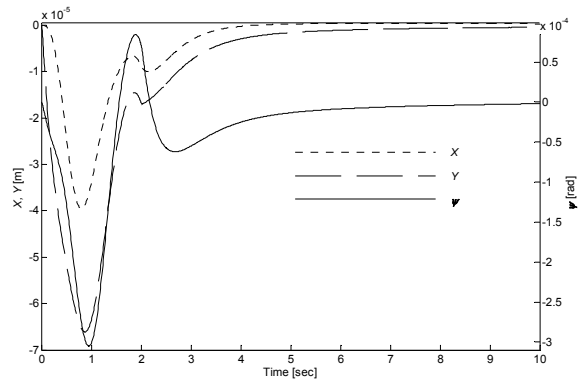


Figure 6: Controlled URV Location Errors

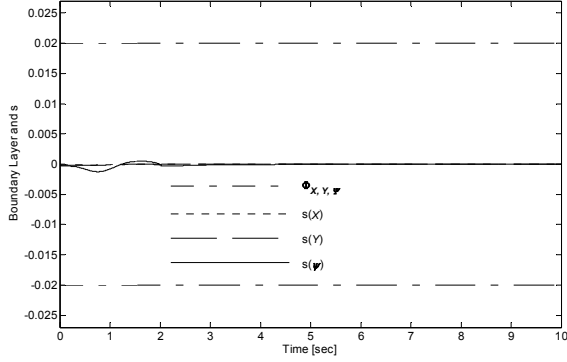


Figure 7: Boundary Layer and s

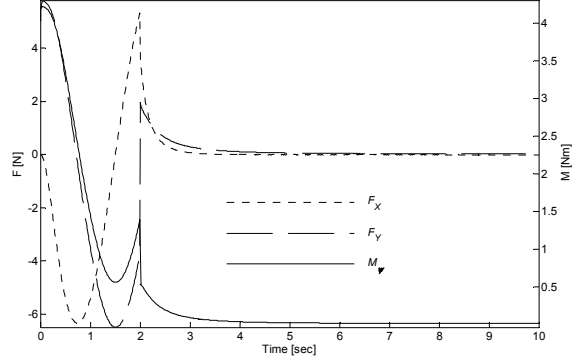


Figure 8: Control Activity

7 CONCLUSION

The incorporation of the AB algorithm into a model-based sliding-mode controller for the reduction of the dynamic coupling between the URV and the manipulator has been accomplished. In order to show the effectiveness of the proposed control scheme, the simulation of a URVM system has been performed and the results have been demonstrated. The simulation results have indicated that the tracking performance of the URVM system is vastly improved by the inclusion of the AB algorithm into the controller. This is consistent with the statement that the desired behaviour can be obtained using the AB modelling strategy in lieu of inertial sensors and the Newton-Euler method. This is due to the fact that the AB approach accounts for the dynamic effects of the manipulator within the URV acceleration equations. Using the Newton-Euler method, inertial measurement are needed to estimate the URV accelerations, which are necessary to compute the dynamical loads of the manipulator on the URV. The AB algorithm affords direct calculation of the URV accelerations based on a known URVM state vector.

ACKNOWLEDGEMENT

The authors wish to thank the Natural Sciences and Engineering Research Council (NSERC) of Canada for providing financial support for this research. The authors also wish to thank Mr. Alp Zibil of the University of Victoria for helping draw Figure 2 and Figure 3.

APPENDIX

URV Parameters:

$$L_0 = 0.596, b_0 = [0 \ 0 \ -0.0254]^T \quad [\text{m}]$$

$$r_{G_0} = [0 \ 0 \ 0]^T \quad [\text{m}]$$

$$m_0 = 32, m_0^f = 32 \quad [\text{kg}]$$

$$I_0 = \text{diag}\{0.498, 0.878, 1.254\} \quad [\text{Nms}^2]$$

$$I_0^A = \text{diag}\{2.654, 3.438, 0.249, 14.9, 18, 115.8\} \quad [\text{Nms}^2]$$

$$A_{x,z} = 0.061 \quad [\text{m}^2]$$

$$C_{0,x,y}^D = 1.07$$

Environmental Parameters:

$${}^E \mathbf{a}_g = [0 \ 0 \ 9.81]^T \quad [\text{m/s}^2]$$

$${}^E \mathbf{a}_f = [0 \ 0 \ 0]^T \quad [\text{m/s}^2]$$

$$\rho = 1000 \quad [\text{kg/m}^3]$$

Manipulator Parameters:

$$L_1 = L_2 = L_3 = 0.22, r_{1,2,3} = 0.0125 \quad [\text{m}]$$

$$\mathbf{b}_{1,2,3} = [0.11 \ 0 \ 0]^T, r_{G_{1,2,3}} = [0.11 \ 0 \ 0]^T \quad [\text{m}]$$

$$r_{G_{1,2,3}} = [0.11 \ 0 \ 0]^T \quad [\text{m}]$$

$$m_{1,2,3} = 1, m_{1,2,3}^f = 1 \quad [\text{kg}]$$

$$I_{1,2,3} = \text{diag}\{0, 0.0137, 0.0137\} \quad [\text{Nms}^2]$$

$$I_0^A = \text{diag}\{0, 0.0017, 0.0017, 0, 0.1078, 0.1078\} \quad [\text{Nms}^2]$$

$$C_{1,2,3}^D = 1.1$$

Control Parameters:

$$b_{r_{\min}} = 1.2870, b_{r_{\max}} = 1.5889, b_{u,v_{\min}} = 36, b_{u,v_{\max}} = 44.44$$

$$\lambda = 3.14 \quad [\text{rad/s}]$$

$$\eta = 0.5, \Phi = 0.02, F_u = 0.5, F_v = 0.5, F_w = 0.5$$

REFERENCES

- [1] M. W. Dunnigan, and G. T. Russell, "Evaluation and reduction of the dynamic coupling between a manipulator and an underwater vehicle," *IEEE Journal of Oceanic Engineering*, vol. 23, no. 3, pp. 260-273, July 1998.
- [2] D. M. Lane, M. W. Dunnigan, P. J. Knightbridge, and A.W. Quinn, "Planning and control for coordination of underwater manipulators," *Proc. IEE Control 91*, pp. 493-498, 1991.
- [3] J. H. Ryu, D. S. Kwon, and P. M. Lee, "Control of underwater manipulators mounted on an roV using base force information," *IEEE International Conference on Robotics & Automation*, pp. 3238-3243, May 2001.
- [4] J. Yuh, "Modeling and control of underwater robotic Vehicles," *IEEE Trans. Syst., Man, Cybern.*, vol. 20, pp. 1475-1483, 1990.
- [5] G. Antonelli, *Underwater robots; Motion and force control of vehicle-manipulator systems*, Springer-Verlag, 2003.
- [6] S. McMillan, "Computational dynamics for robotic systems on land and underwater," *Ph.D Dissertation*, The Ohio State University, Columbus, Summer 1994.
- [7] D. Yoerger, and J. J. E. Slotine, "Robust trajectory control of underwater vehicles," *IEEE J. Oceanic Eng.*, vol. OE-10, pp. 462-470, Oct. 1985.
- [8] K. Ioi, and K. Itoh, "Modeling and simulation of an underwater manipulator," *Advanced Robotics*, vol. 4, no. 4, pp. 303-317, 1990.
- [9] S. McMillan, D. E.Orin, and R. B. McGhee, "Efficient dynamic simulation of an underwater vehicle with a robotic manipulator," *IEEE Trans. Syst., Man, Cybern.*, vol. 25 pp. 1194-1206, Aug. 1995.
- [10] T. J. Tarn, G. A. Shoults, and S. P. Yang, "A dynamic model of an underwater vehicle with a manipulator using Kane's method," *J.Autonomous Robots*, vol. 3, no. 2, pp. 195-209, June/July 1996.
- [11] J. J. Craig, *Introduction to Robotics, 2nd Edition*. Addison-Wesley, 1989.
- [12] T. I. Fossen, *Guidance and Control of Ocean Vehicles*, John Wiley&Sons, 1994.
- [13] M. H. Patel, *Dynamics of Offshore Structures*, Butterworths, 1989.
- [14] J. N. Newman, *Marine Hydrodynamics*, MIT Press, 1977.
- [15] B. Levesque, and M. J. Richard, "Dynamic analysis of a manipulator in a fluid environment," *Int J Robotics Res.*, vol. 13, pp 221-213, 1994.
- [16] D. R. Yoerger, J. G. Cooke, and J. J. E. Slotine, "The influence of thruster dynamics on underwater vehicle behaviour and their incorporation into control system design," *IEEE J. Oceanic Eng.*, vol. 15, no. 3, pp. 167-177, July 1990.
- [17] W. P. A. Van Lammeren, J. D. Van Manen, and M. W. C. Oosterveld, "The Wageningen B-screw series," *Trans., ASME*, pp. 269-317, Nov. 1969.
- [18] J. Healey, S. M. Rock, S. Cody, D. Miles, and J. P. Brown, "Toward an improved understanding of thruster dynamics for underwater vehicles," *IEEE J. Oceanic Eng.*, vol. 20, pp. 354-361, Oct. 1995.
- [19] R. Bachmayer, L. L. Whitcomb, and M. Grosenbaugh, "An accurate four-quadrant nonlinear dynamical model for marine thrusters: theory and experimental validation," *IEEE J. Oceanic Eng.*, vol. 1, no. 25, pp. 146-159, Jan. 2000.
- [20] R. Featherstone, "The calculation of robot dynamics using articulated-body inertias," *Int. J. Robotics Research*, vol. 2, no. 1, pp. 89-104, 1983.
- [21] R. Cristi, F. A. Papoulias, A. J. Healey, "Adaptive sliding mode control of autonomous underwater vehicles in the dive plane," *IEEE J. Oceanic Eng.*, vol. 15, no. 3, pp. 152-160, July 1990.
- [22] J. J. E. Slotine, and L. Weiping, *Applied Nonlinear Control*, Prentice-Hall, 1991.